Active Control and Excitation of Breathing Oscillations in a Hall Thruster with a Fast Digital Signal Processor

IEPC-2013-339

Presented at the 33rd International Electric Propulsion Conference,
The George Washington University, Washington, D.C., USA
October 6–10, 2013

S. Barral,[*] J. Kaczmarczyk[†] and J. Kurzyna[‡]
Institute of Plasma Physics and Laser Microfusion, 01-497 Warsaw, Poland

and

M. Dudeck[§]
Université Pierre et Marie Curie - Paris 6, 75252 Paris Cedex, France

An experimental characterization of Hall thruster current discharge oscillations when moderate levels of oscillations are superimposed on the discharge voltage is performed in both open loop and closed loop configurations. Investigations of the dynamic behavior up to 200 kHz were made possible by the use of a custom-designed high power voltage regulator and a strongly optimized digital controller implementation on a fast digital signal processor. This new experiment with proportional-integral-derivative control has confirmed the authors' earlier findings that proportional (resistive) control provides very large damping of breathing oscillations at low voltages, although its effectiveness decreases at high voltages. The destabilizing effect of positive feedback was also studied and confirmed for pure proportional, integral and derivative feedback. Open loop operation shows, in turn, a very clear resonance around 20 kHz, while its gain and phase behaviors present striking similarities with those of the predator-prey model of breathing oscillations.

I. Introduction

Although active control of oscillations in Hall thrusters was initially prompted by the stabilization of clustered propulsion systems,[1] it While such investigations are of great interest to establish correlations with theoretical[2] of numerical[3] models of oscillations, other motivations exist such as the hypothetical possibility to achieve larger efficiency or decreased divergence, the reduction of EMI radiated to the payload or the generation of very stable operating conditions mandated by some experimental measurements. With a goal related to the latter, other experiments have on the contrary sought to generate stable oscillations using open loop control.[4,5,6]

Unlike passive control strategies targeting breathing oscillations[7] or spoke oscillations,[8] active control acts on the process in real time and must thus resolve the characteristic time scale of the phenomenon, which in the case of breathing and spoke oscillations is the $10 - 100\,\mathrm{kHz}$ range. In the simplest setup, passive electronic components can be used to modulate the discharge voltage as a function of the discharge current. This solution is, in fact, commonly adopted in commercial Hall thrusters where a LC or RLC networks is set in series with the discharge.[9,10,11,12] This approach was also adopted for the active control of spoke oscillations where a pure resistive network.[13] The authors have investigated another method, however, based on a custom analog proportional-integral-derivative (PID) controller.[14] Electronic control offers much

*Research associate, Division of Magnetized Plasmas, serge.barral@ipplm.pl.
†Research engineer, Division of Magnetized Plasmas, jacek.kacmzarczyk@ipplm.pl.
‡Research associate, Division of Magnetized Plasmas, jacek.kurzyna@ipplm.pl.
§Professor, Institut Jean le Rond d'Alembert, dudeck@ida.upmc.fr.

greater flexibility since the controller's constants can be changed on the fly without hardware modification. It is also characterized by a much greater power efficiency for engineering applications since resistive control is only applied to the *ac* component of the current, avoiding thus the large Joule losses associated to the *dc* current[a].

The present work goes one step further in terms of flexibility and performance with a controller based on a digital signal processor (DSP), which allows not only the feedback parameters to be modified but also enables the implementation of a variety of control algorithms and filters without hardware change.

II. Controller architecture

A. Overview

The controller is built around a dual-core hybrid microcontroller/DSP and a high power voltage regulator, which generate controlled oscillations of the discharge voltage based on signal processing of the discharge voltage.

The experimental setup is schematically depicted in Fig. 1. The second processing core (core B) takes the discharge current measured by an analog-to-digital converter (ADC) as input, and drives the voltage regulator through a digital-to-analog converted (DAC). Serial communication with the terminal is handled by the first processing core (core A) and realized via optical fibers. Optical communication ensures electrical insulation between the terminal and the controller, as the latter is by design on the positive side of the power supply. Core A pre-processes and forwards to core B all instructions issued by the terminal, such as changes of the PID constants, changes of the digital filter parameters, requests for data, etc. This architecture allows core B to be fully dedicated to signal processing and warrant real-time, deterministic processing: the processing of each discharge current sample is guaranteed to be completed before the next sample is available, even in the event the PID controller constants are being changed or a request for data is being issued.

The voltage regulator is connected in series with the power supply. Owing to the relatively high frequency of operation, a linear voltage regulator is used instead of a switched-mode regulator, meaning that only voltage drops can be generated. For this reason, if one wants to impose voltage oscillations of amplitude V_{ac} around a fixed value V_0, it is necessary to set the power supply at a slightly higher voltage $V_0 + V_b$ where V_b is a fixed bi as voltage, and to have the regulator generate a potential drop equal to $V_b - V_{ac}$. The value of V_b must be therefore chosen greater than the highest value expected for V_{ac}.

In order to improve the stability of the reference voltage $V_0 + V_b$, a large reservoir capacitor of $18.2\,\mu$F is connected in parallel with the power supply.

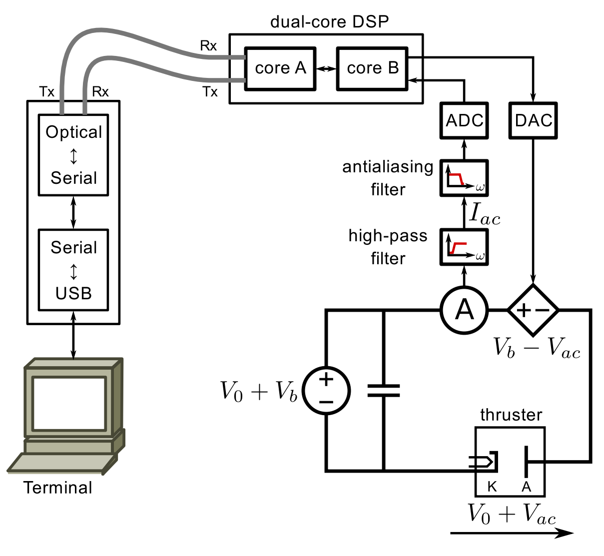

Figure 1: Simplified schematic of the experimental setup.

[a]In theory, a switched-mode regulator could as well eliminate *ac* losses, but very high switching frequencies above 1 MHz would be required for this approach to become practical.

B. DSP and analog-digital converters

The Blackfin BF561, a 32 bits dual-core processor with fixed-point DSP capabilities, was used for signal processing. Although its clock rate was set to 500 MHz (the rated maximum being 600 MHz), its ability to process up to 3 parallel instructions per core and per cycle make it a very compelling option for fast digital processing. Blackfin processors are also very well supported by the free GCC compiler and if needed can run a variety of operating system, including uClinux.

Because of the stringent scheduling requirements for core B, however, it would be probably impossible even for a real-time operating system to meet the latency requirements associated with the processing of a signal sampled at 1.25 MS/s. For this reason, the controlling algorithm, written in C and in assembly for critical sections, run directly on the processor hardware without operating system. Although core A could in principle run an operating system, it needs to access directly serial port hardware and specific memory blocks for which custom drivers would be required; it was therefore decided to also run core A without operating system.

The ADC and DAC directly communicate with the processor via serial and parallel interfaces, respectively. Both have 12 bits precision and were operated at 1.25 MS/s, which means that up to 400 clock cycles are available to process each samples. An optional Butterworth anti-aliasing filter with a cutting frequency at 500 MHz was used at the input of the ADC. Although no aliasing effects were observed, for the sake of precaution the anti-aliasing filter was systematically used in all experiments.

C. Voltage regulator

The voltage regulator is similar in design to the former MOSFET-based regulator.[15] Its performances have been significantly improved, however, both in terms of bandwidth (200 kHz *vs* 100 kHz) and voltage range ($\pm$25 V *vs* $\pm$8 V). A constant internal bias voltage of about $V_b \approx 28$ V is applied, meaning that as V_{ac} varies within the range $\pm$25 V, the voltage drop generated by the regulator varies between 3 V and 53 V.

III. PID algorithm

A. Principle

The PID feedback loop is shown in Fig. 2. As in previous experiments, only the *ac* component I_{ac} of the discharge current is processed and a constant setpoint voltage V_0 is added to the zero-average voltage V_{ac} computed by the PID. Although in a canonical PID implementation a setpoint current I_0 would be prescribed and the total discharge voltage would be computed directly based on the error $I - I_0$, such feedback loop would be prone to instabilities as Hall thrusters often exhibit zero or even negative *dc* resistance.

Even though in theory the integral term should show no long-term drift ("integral windup") since the input I_{ac} is a zero-average value, in practice hardware imperfections and digital quantization are likely to generate long term drifts in the integral output. For this reason, the integral term is composed with a 2^{nd}-order high-pass filter which frequency was set to 5 kHz in all experiments.

The derivative term is prone to generate high frequency noise and, due to technical reasons, may also generate a negative feedback instability in the linear regulator. For this reason, it is composed with a 2^{nd}-order low-pass filter which frequency was set to 60 kHz in all experiments.

B. Digital implementation

Both 2^{nd}-order digital filters are Infinite Impulse Response (IIR) filters. This enables each of the 3 PID blocks, namely the proportional, integral+high-pass, derivative+low-pass blocks, to be put in the form of a digital biquad with a Z-transform of the type:

$$H(z) = \frac{b_0 + b_1 z^{-1} + b_2 z^{-2}}{1 + a_1 z^{-1} + a_2 z^{-2}},$$

which use a Direct Form I implementation. Much care has been taken to pre-shift and post-shift registers as appropriate to avoid as much as possible round-off errors. Each coefficient is stored in a 16-bits fractional format, and the results of all multiplications are stored in 32-bits registers, using as well 40-bits registers for intermediate steps to ensure that all computations are saturating (*i.e.* that overflow result in the largest possible value and not in an artifact).

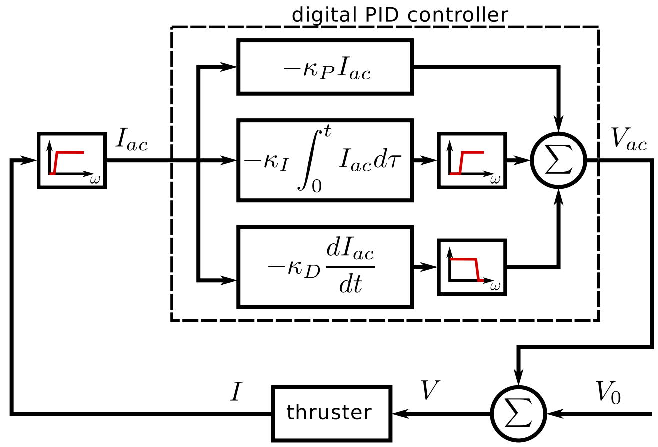

Figure 2: Schematic of the PID feedback loop.

Later subsections provide the Z-transform for each block.

1. *Proportional block*

The proportional term composed with a low-pass filter has a transform of the type:

$$\tilde{H}_P \tilde{H}_L(z) = \tilde{\kappa}_P \frac{\omega_L^2 \left(1 + 2z^{-1} + z^{-2}\right)}{\left(\omega_L^2 + 2\frac{\omega_L}{Q} + 4\right) + 2\left(\omega_L^2 - 4\right) z^{-1} + \left(\omega_L^2 - 2\frac{\omega_L}{Q} + 4\right) z^{-2}}.$$

Note, however, that the filter of the proportional term proved unnecessary and was disabled in all experiments.

2. *Integral block*

The integral term composed with a high-pass filter has a transform of the type:

$$\tilde{H}_I \tilde{H}_H(z) = \tilde{\kappa}_I \frac{2\left(1 - z^{-2}\right)}{\left(\omega_H^2 + 2\frac{\omega_H}{Q} + 4\right) + 2\left(\omega_H^2 - 4\right) z^{-1} + \left(\omega_H^2 - 2\frac{\omega_H}{Q} + 4\right) z^{-2}}$$

3. *Derivative block*

The derivative term composed with a low-pass filter has a transform of the type:

$$\tilde{H}_D \tilde{H}_L(z) = \tilde{\kappa}_D \frac{2\omega_L^2 \left(1 - z^{-2}\right)}{\left(\omega_L^2 + 2\frac{\omega_L}{Q} + 4\right) + 2\left(\omega_L^2 - 4\right) z^{-1} + \left(\omega_L^2 - 2\frac{\omega_L}{Q} + 4\right) z^{-2}}$$

4. *Optimized code*

The optimized, hand-written assembly implementation of the PID is provided in appendix. The processing of an ADC value up to the transfer of the PID output to the DAC takes only 38 clock cycles, which means that the processing delay is less than 80 ns and provide for a theoretical maximum sampling rate an order of magnitude above the sampling rate used in this experiment.

IV. Results and discussion

Experiments were performed in Orléans (France) in the PIVOINE facility of the ICARE laboratory (CNRS), using the PPS-100ML laboratory Hall thruster. The vessel pressure was kept lower than 2×10^{-5} mbar in all cases.

A. Closed loop PID operation

1. *Parametrical exploration of the PID settings*

A parametrical study has been performed at $V_0 = 148\,\mathrm{V}$ and $V_0 = 297\,\mathrm{V}$ by changing each of the PID setting individually within the range $\kappa_P = -16 \div 32\,\Omega$, $\kappa_I = -3.2 \times 10^6 \div 3.2 \times 10^6\,\mathrm{F}^{-1}$ and $\kappa_D = -208 \div 208\,\mu\mathrm{H}$, as shown in Figs 3 and 4. Simultaneous changes of the different PID settings have been attempted but were not found to provide any improvement over pure proportional control.

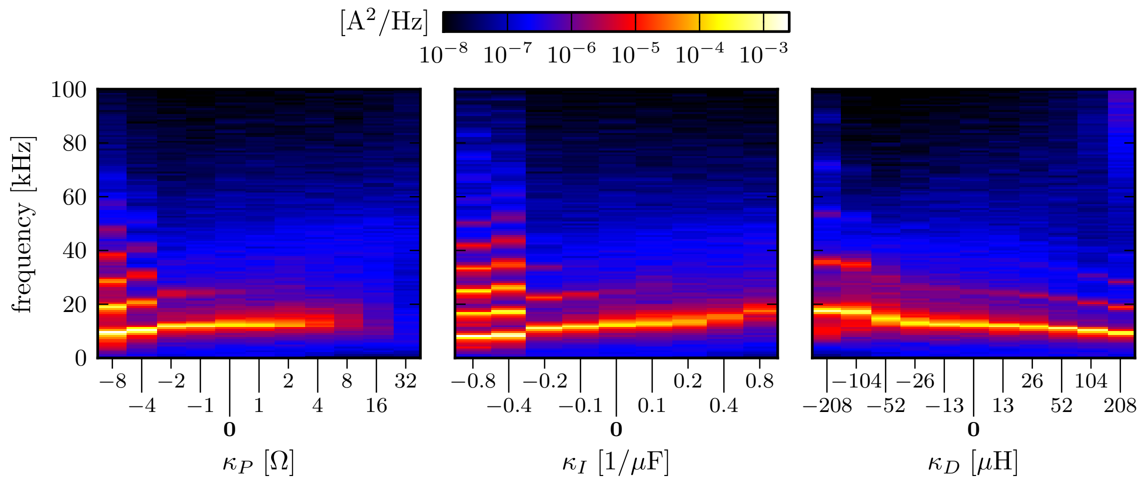

Figure 3: Power spectral density of the discharge current. Parametrical exploration of the effect of pure proportional, integral and derivative control at $V_0 = 148$ V with an anode mass flow rate of $3.5\,\mathrm{mg\,s^{-1}}$.

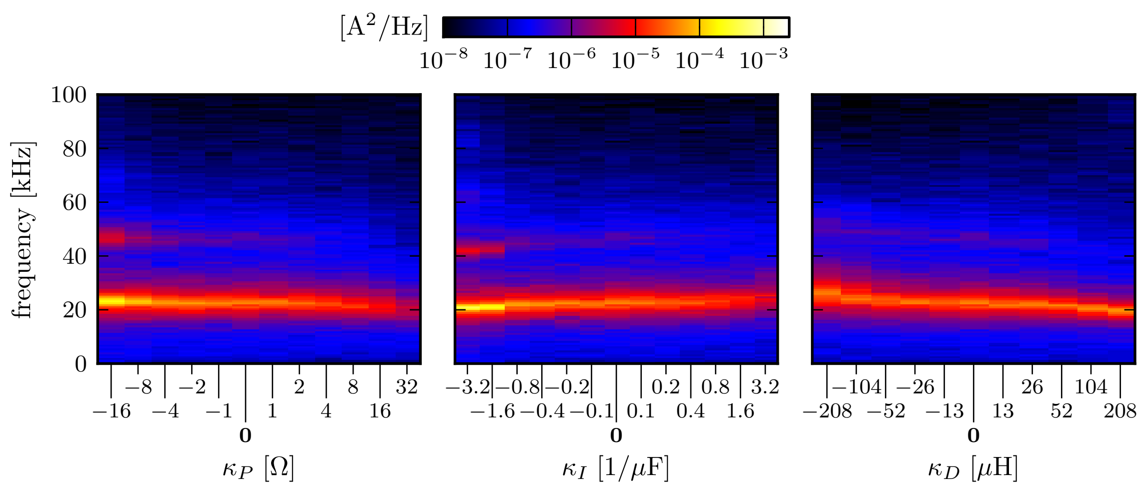

Figure 4: Power spectral density of the discharge current. Parametrical exploration of the effect of pure proportional, integral and derivative control at $V_0 = 297$ V with an anode mass flow rate of $3.5\,\mathrm{mg\,s^{-1}}$.

As observed in our earlier experiments,[15] PID control was found most effective at low discharge voltages. Proportional control was much more efficient than integral control, while derivative control does not appear to bring any significant improvement. Beside the large increase in the PID constant range, the new controller also enables exploration with negative settings, *i.e.* positive feedback. The destabilizing effect of positive feedback was observed with all 3 types of control, generating very wide oscillations with strong non-linear features (pulse-like shape) as testified by the many harmonics visible in the power spectra. The fact that integral control provides some damping, albeit moderate, is an improvement over our former experiments where integral control was affected by low frequency instabilities. These instabilities appear to have been effectively canceled by the digital 2^{nd}-order filter of the integral block.

2. *Voltage exploration*

A proportional gain of $\kappa_P = 16\,\Omega$ was selected for the first discharge voltage exploration as further increases in gain did not provide significant improvements and could in some cases exceed the linear range of the voltage regulator, resulting in voltage clamping at the ± 25 V rails.

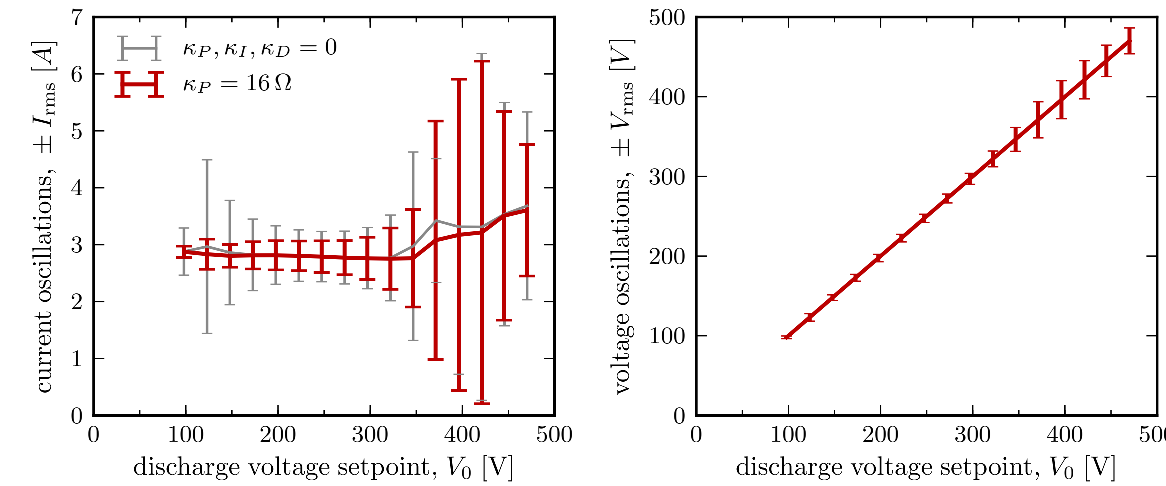

(a) Current oscillations, $\kappa_P = 0$ *vs* $\kappa_P = 16\,\Omega$. (b) Voltage oscillations, $\kappa_P = 16\,\Omega$.

Figure 5: (a) Average discharge current and oscillation amplitude (summed over the whole frequency spectrum) at various voltage setpoints with and without proportional control with an anode mass flow rate of $3.5\,\mathrm{mg\,s^{-1}}$ and (b) corresponding voltage oscillations around the setpoint voltage with proportional control.

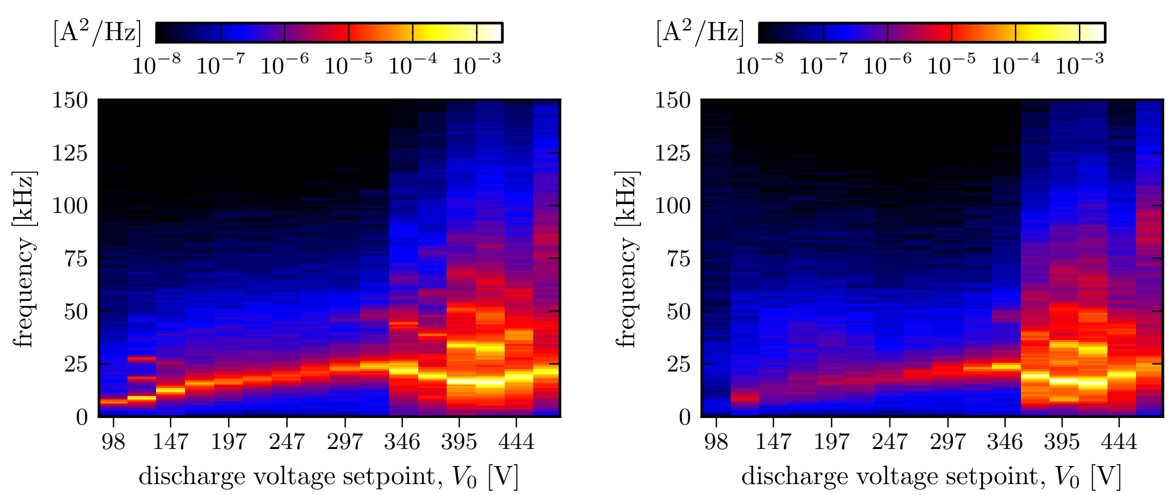

(a) $\kappa_P = \kappa_I = \kappa_D = 0$ (b) $\kappa_P = 16\,\Omega, \quad \kappa_I = \kappa_D = 0$

Figure 6: Power spectral density of the discharge current at various voltage setpoints with and without proportional control with an anode mass flow rate of $3.5\,\mathrm{mg\,s^{-1}}$.

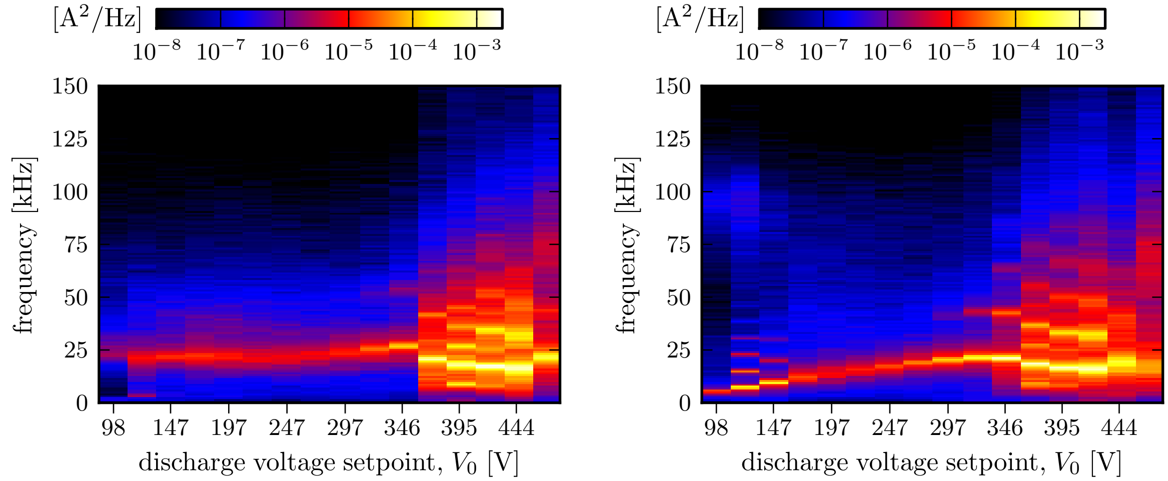

(a) $\kappa_I = 2 \times 10^6\,\mathrm{F}^{-1}, \quad \kappa_P = \kappa_D = 0$

(b) $\kappa_D = 125\,\mu\mathrm{H}, \quad \kappa_P = \kappa_I = 0$

Figure 7: Power spectral density of the discharge current at various voltage setpoints with pure integral and pure derivative control with an anode mass flow rate of $3.5\,\mathrm{mg\,s^{-1}}$.

Although it was hoped that the much wider voltage range of the new controller may improve control at high voltages (below 300 V), it turned out impossible to improve the situation in the space-charge saturated sheath regime.[16,17] The dramatic effect of proportional control can be appreciated, however, by looking and at the overall reduction of oscillations at low voltages on Fig. 5 and by comparing the frequency spectra with and without proportional control on Fig. 6.

Similar explorations were performed with pure integral and derivative control (Fig. 7), which confirmed the moderate ability of integral control to damp oscillations and the inability of derivative control to do so.

B. Open loop operation

1. Description

Advantage was taken from the fact that the controller can be reprogrammed to act as a high power signal generator. A sinusoidal voltage wave V_{ac} of amplitude ± 10 V peak-to-peak was thus generated on top of the constant setpoint voltage V_0, and the response in terms of discharge current was measured. Synchronous measurement enables the derivation of both the gain and phase of the open loop transfer function for such forced oscillations. The method is relatively close to that adopted by other authors[4,5,6] where the cathode keeper was biased at an oscillating voltage. It can be argued, however, that the present method is conceptually simpler to interpret as is does not rely on the complex physics of hollow cathodes and on the engineering details of its construction. It is very likely, however that variations in the keeper voltage actually result in variations in the coupling voltage between the cathode and the plume, meaning it is equivalent to varying the voltage across the plasma column as was done here.

It must be underlined that the measurement where done at higher voltage ($V_0 = 347$V) and with a different magnetic field settings than in section A. This operating point was chosen because it was characterized by a very small level of oscillations, which simplified the subtraction of the background signal from the signal due to forced voltage oscillations.

2. Experimental Bode plots

The gain of the transfer function was computed by integrating the spectral power of discharge oscillations in a narrow ± 500 Hz window around the forcing frequency. After this, the background, *i.e.* the spectral power in the same frequency window from the case without forced oscillations, was subtracted to obtain the power due to the forced oscillations only. It was found that, even though the window width affected the total power in the raw signal, it had nearly no influence on the residual signal once the background was subtracted.

The phase was computed by cross-correlation between the time series of the forcing discharge voltage and the response of the discharge current.

The Bode plots of Fig. 8 show a very clear resonance at the breathing frequency, which qualitatively corroborates the findings of Dannenmayer *et al.*[4,5] The general low-ω and high-ω behavior point to a 2^{nd}order band-pass like behavior, with the phase switching from $\approx \pi/2$ to $-\pi/2$ as the resonance is crossed. The high-frequency behavior of the gain appears somewhat unusual, though, since despite the phase switch to $-\pi/2$, gain shows a plateau in the $50-100$ kHz range. The plateau behavior remains unexplained; it is surmised, however, that it could relate to the ion transit-time mode which is usually excited in this precise frequency range, although the non-excited frequency spectrum of the discharge current at this operating point does not hint a the presence of transit-time oscillations.

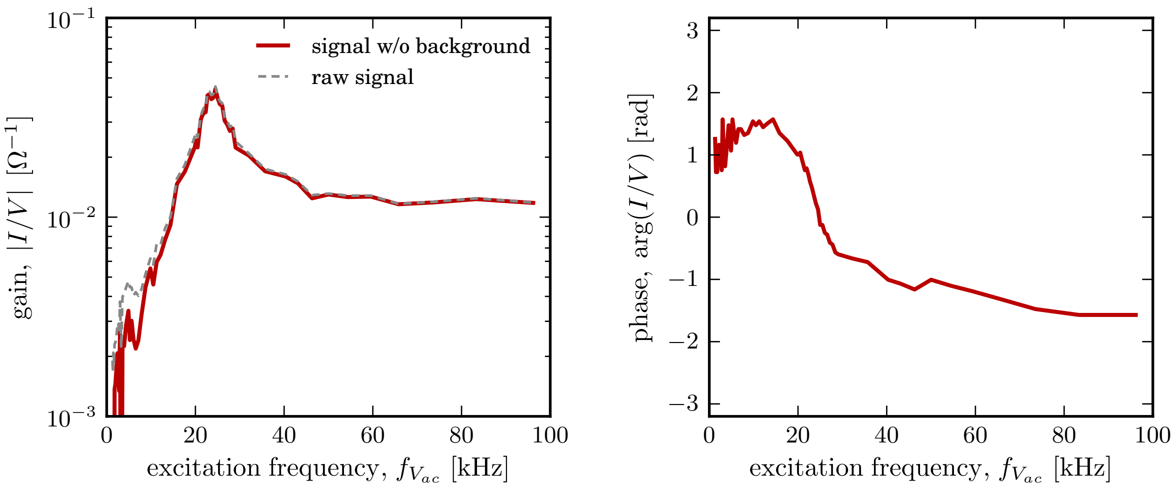

(a) Gain. (b) Phase

Figure 8: Bode plots of the discharge current response to forced sinusoidal oscillations of the discharge voltage (± 10 V peak-to-peak). A quiet operating point with low levels of natural oscillations was chosen ($V_0 = 347$ V and $\dot{m} = 4.8\,\mathrm{mg\,s^{-1}}$).

3. Theoretical Bode plots

The measured open loop transfer function were compared against those obtained from the predator-prey theory of breathing oscillations. The theory is outlined in a number of papers.[18,19,20,21,2] The most tractable and realistic model for the case at hand is the time-delayed model,[21] which can be easily augmented with a voltage-dependent term as outlined in an earlier work.[19] This leads to the dynamical system:

$$\frac{dI}{dt} = \beta_N I \left(N - \bar{N}\right) + \beta_V I \left(V - \bar{V}\right), \quad (1)$$

$$\frac{dN}{dt} = -\gamma I N + \frac{Q_0}{L} \exp\left(-\gamma \int_{t-\tau}^{t} I dt\right), \quad (2)$$

where I is the discharge current, N the density of neutrals, V is the discharge voltage (where overbars indicate steady-state value), Q_0 the propellant flow rate, τ is the transit-time of neutrals in the pre-ionization zone, β_N and β_V are effective ionization rates (*birth rates*) that account for variations in terms of neutrals density and voltage, respectively, and γ is the depletion rate for neutrals (*death rate*).

Performing a small perturbation analysis, one can derive the following transfer function:

$$\frac{\hat{I}}{\hat{U}} = R_0^{-1} \frac{\jmath \frac{\omega}{\omega_c} + \sqrt{\epsilon}}{\jmath \frac{\omega}{\omega_c}\left(\jmath \frac{\omega}{\omega_c} + \sqrt{\epsilon}\right) + \left\{1 + \frac{\omega_c}{\jmath \omega} \frac{1}{\sqrt{\epsilon}} \left[1 - \exp\left(-\jmath \omega \tau\right)\right]\right\}}, \quad (3)$$

where:

$$\epsilon \equiv \frac{\gamma \bar{I}}{\beta_N \bar{N}} \ll 1, \tag{4}$$

$$\omega_c \equiv \sqrt{\beta_N \gamma \bar{I} \bar{N}}, \tag{5}$$

$$R_0 \equiv \frac{\omega_c}{\bar{I}\beta_V}. \tag{6}$$

Since the nominal point is very quiet in the breathing frequency range, the mode can be considered stable and the time delay small.[21] By neglecting time delay altogether ($\tau = 0$), the shape of the bode plots becomes solely determined by ϵ since the resistance R_0 and the oscillator eigenfrequency ω_c only determines the scaling on the gain and frequency axes. Except for the above-mentioned plateau, a very good agreement with experimental bode plots is found, as shown in the theoretical bode plots of Fig. 9.

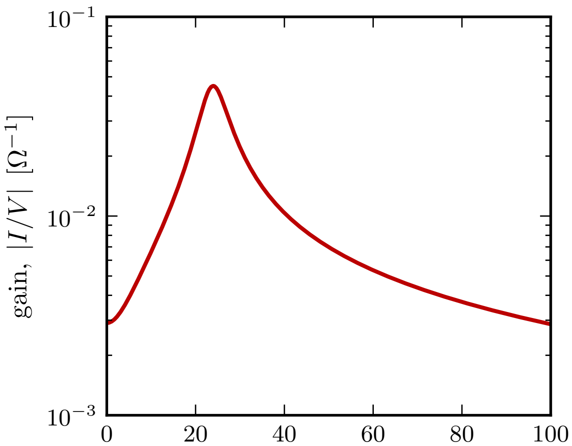

(a) Gain.

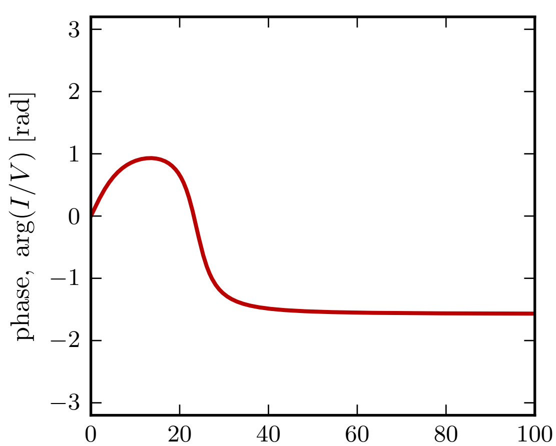

(b) Phase

Figure 9: Theoretical bode plots for the predator-prey model, based on the transfer function of Eq. 3 with $\tau = 0$ and $\epsilon = 1/15$. Parameters ω_c and

V. Conclusion

Many of the authors' earlier finding have been recovered, including the difficulty to stabilize high voltage operation once the space charge saturated regime is entered. Improved filtering with digital filters have enabled, however, proper operation of the pure integral control mode which even demonstrated a small but noticeable damping of current oscillations. Positive feedback control was found to strongly enhance oscillations whether it is applied with pure proportional, integral or derivative control.

Although more limited in scope, open loop investigations appear very promising due to the possibility to compare transfer functions directly with theoretical models, which provides one of the most direct link so far between experiment and predator-prey theory. Preliminary comparisons between experimental and theoretical bode plots are very encouraging, with phase behaviors in near-perfect agreement. A discrepancy is observed for the gain behaviors at frequencies above 50 kHz which could be due to the fact that other oscillatory modes are at play, but the theoretical and experimental gain behaviors below this threshold are remarkably similar.

Acknowledgments

This work has been performed with the support of the French Research Group "Propulsion par plasma dans l'espace" (GDR 3161 CNRS/CNES/SNECMA/Universités). The authors wish to thank the Pivoine staff and in particular Guillaume Largeau and Guillaume Daniel for their assistance.

Appendix: PID biquad kernel

```
/*
   The 15 coefficients of the P, I, D biquads are stored contiguously in memory.
   The I0 register is initialized to point to the last coefficient of the D biquad.

   The previous 2 values of the discharge current read by the ADC are stored
   contiguously in memory. The I1 register is initialized to points to the
   oldest of those 2 values.

   The previous 2 values of the voltage computed by each of the P, I and D
   biquads (6 values in total) are stored contiguously in memory. The P0
   register is initialized to points to the first value (newest value of P).

   The I2 register points to the ADC.
   The P1 register points to the DAC.
*/

// Wait for an ADC interrupt and Load the 12 bit ADC value as a fract16 value.
IDLE;
R6.L=W[I2];
R6<<=4;

/* Compute the derivative term (saturating). Equivalent code:
    y0D = -a1D*y1D -a2D*y2D + b0D*x0 + b1D*x1 + b2D*x2;
    y2D = y1D;
*/
MNOP           || R0.L=W[I0--]   || R1.L=W[I1--];
A0=R0.L*R1.L   || R0.L=W[I0--]   || R1.L=W[I1++];
A0+=R0.L*R1.L  || R0.L=W[I0--];
A0+=R0.L*R6.L  || R0.L=W[I0--]   || R1=[P0+20];
A0=A0<<3;
A0+=R0.L*R1.H, A1=R0.L*R1.L (M)  || R0.L=W[I0--] || R1=[P0+16];
A0+=R0.L*R1.H, A1+=R0.L*R1.L (M) || [P0+20]=R1;
A1=A1>>>15;
R2=(A0+=A1)    || R0.L=W[I0--]   || R1.L=W[I1--];
R2=R2<<1 (S);

/* Compute the integral term (saturating). Equivalent code:
    y1D = y0D;
    y0I = -a1I*y1I -a2I*y2I + b0I*x0 + b1I*x1 + b2I*x2;
    y2I = y1I;
*/
A0=R0.L*R1.L   || R0.L=W[I0--]   || R1.L=W[I1++];
A0+=R0.L*R1.L  || R0.L=W[I0--]   || [P0+16]=R2;
A0+=R0.L*%0.L  || R0.L=W[I0--]   || R1=[P0+12];
A0=A0>>>3;
A0+=R0.L*R1.H, A1=R0.L*R1.L (M)  || R0.L=W[I0--] || R1=[P0+8];
A0+=R0.L*R1.H, A1+=R0.L*R1.L (M) || [P0+12]=R1;
A1=A1>>>15;
R2=(A0+=A1)    || R0.L=W[I0--]   || R1.L=W[I1--];
R2=R2<<1 (S);

/* Compute the proportional term (saturating). Equivalent code:
    y1I = y0I;
    y0P = -a1P*y1P -a2P*y2P + b0P*x0 + b1P*x1 + b2P*x2;
```

```
    y2P = y1P;
*/
A0=R0.L*R1.L   || R0.L=W[I0--]   || R1.L=W[I1];
A0+=R0.L*R1.L  || R0.L=W[I0--]   || [P0+8]=R2;
A0+=R0.L*%0.L  || R0.L=W[I0--]   || R1=[P0+4];
A0+=R0.L*R1.H, A1=R0.L*R1.L (M)  || R0.L=W[I0--] || R1=[P0];
A0+=R0.L*R1.H, A1+=R0.L*R1.L (M) || [P0+4]=R1;
A1=A1>>>15;
R2=(A0+=A1);
R2=R2<<1 (S)   || R1=[P0+8];

/* Compute the PID output y0=y0P+y0I+y0D (saturating). Equivalent code:
    x2 = x1;
    x1 = x0;
    y0=y0P+y0I+y0D;
*/
A0=R2          || [P0]=R2;
A1=R1          || R2=[P0+16]     || R1.L=W[I1++];
A0+=A1         || W[I1--]=R1.L;
A1=R2          || W[I1++]=%0.L;
R1=(A0+=A1);

/* Set y0=16*y0 as a fract16 value and set the 12-bit DAC value
   to the unsigned short (y0+1)*16*2^12
*/
R3.L=R1.H<<4 (S);
R0.L=R3.L>>4;
BITTGL(R0, 11);
W[P1]=R0.L;
```

References

[1]Lobbia, R. B. and Gallimore, A. D., “Evaluation and Active Control of Clustered Hall Thruster Discharge Oscillations,” *Proc. 41st AIAA Joint Propulsion Conference*, No. 2005-3679, American Institute of Aeronautics and Astronautics, Washington, D.C., Tucson, AZ, 2005.

[2]Barral, S. and Peradzyński, Z., “Ionization Oscillations in Hall Accelerators,” *Phys. Plasmas*, Vol. 17, 2010, pp. 014505.

[3]Barral, S. and Miedzik, J., “Numerical Investigation of Closed-Loop Control for Hall Accelerators,” *J. Appl. Phys.*, Vol. 109, 2011, pp. 013302.

[4]Dannenmayer, K., Kudrna, P., Tichý, M., and Mazouffre, S., “Time-Resolved Measurement of Plasma Parameters in the Far-Field Plume of a Low-Power Hall Effect Thruster,” *Plasma Sources Sci. Technol.*, Vol. 21, 2012, pp. 055020.

[5]Dannenmayer, K., Kudrna, P., Tichý, M., and Mazouffre, S., “Time-Resolved Measurements of Plasma Properties Using Electrostatic Probes in the Cross-Field Discharge of a Hall Effect Thruster,” *Contrib. Plasma Phys.*, Vol. 53, 2013, pp. 63.

[6]Vaudolon, J., Balika, L., and Mazouffre, S., “Photon Counting Technique Applied to Time-Resolved Laser-Induced Fluorescence Measurements on a Stabilized Discharge,” *Rev. Sci. Instrum.*, Vol. 84, 2013, pp. 073512.

[7]Tamida, T., Nakagawa, T., Suga, I., Osuga, H., Ozaki, T., and Matsui, K., “Determining Parameter Sets for Low-Frequency-Oscillation-Free Operation of Hall Thruster,” *J. Appl. Phys.*, Vol. 102, 2007, pp. 043304.

[8]Ellison, C. L., Raitses, Y., and Fisch, N. J., “Cross-Field Electron Transport Induced by a Rotating Spoke in a Cylindrical Hall Thruster,” *Phys. Plasmas*, Vol. 19, No. 1, 2012, pp. 013503.

[9]Kim, V., Kozlov, V., Popov, G., and Skrylnikov, A., “Investigation of the Stationary Plasma Thruster Scale Impact on the Electric Filter Parameter Choice,” *Proc. 26th International Electric Propulsion Conference*, No. 99-119, The Electric Rocket Propulsion Society, Worthington, OH, Kitakyushu (Japan), 1999.

[10]Mikhailichenko, V. A., Morozov, A. I., Smirnov, V. A., and Tilinin, G. N., “Investigation of "Contour" Oscillations in Accelerators with Closed Electron Drift and Extended Acceleration Zone,” *Proc. 2nd All-Union Conference on Plasma Accelerators and Ion Injectors*, Minsk, 1973, p. 12, In Russian.

[11]Zhurin, V. V., Kaufman, H. R., and Robinson, R. S., “Physics of Closed Drift Thrusters,” *Plasma Sources Sci. Technol.*, Vol. 8, 1999, pp. R1–R20.

[12]Lobbia, R. B. and Gallimore, A. D., “Dynamic Electromagnetic Field Measurements of Clustered Hall Thrusters,” *Proc. 42nd AIAA Joint Propulsion Conference*, No. 2006-4996, American Institute of Aeronautics and Astronautics, Washington, D.C., Sacramento, CA, 2006.

[13]Griswold, M. E., Ellison, C. L., Raitses, Y., and Fisch, N. J., "Feedback Control of an Azimuthal Oscillation in the E×B Discharge of Hall Thrusters," *Phys. Plasmas*, Vol. 19, No. 1, 2012, pp. 053506.

[14]Barral, S., Kaczmarczyk, J., Kurzyna, J., and Dudeck, M., "Active Control of a Hall Thruster Discharge," *Proc. 32nd International Electric Propulsion Conference*, No. 11-193, The Electric Rocket Propulsion Society, Worthington, OH, Wiesbaden (Germany), 2011.

[15]Barral, S., Kaczmarczyk, J., Kurzyna, J., and Dudeck, M., "Closed-Loop Control of Ionization Oscillations in Hall Accelerators," *Phys. Plasmas*, Vol. 18, 2011, pp. 083504.

[16]Barral, S., Makowski, K., Peradzyński, Z., Gascon, N., and Dudeck, M., "Wall Material Effects in Stationary Plasma Thrusters. II. Near-Wall and In-Wall Conductivity," *Phys. Plasmas*, Vol. 10, 2003, pp. 4137.

[17]Gascon, N., Dudeck, M., and Barral, S., "Wall Material Effects in Stationary Plasma Thrusters. I. Parametric Studies of an SPT-100," *Phys. Plasmas*, Vol. 10, 2003, pp. 4123.

[18]Fife, J. M., Martínez-Sánchez, M., and Szabo, J., "A Numerical Study of Low-Frequency Discharge Oscillations in Hall Thrusters," *Proc. 33rd AIAA Joint Propulsion Conference*, No. 97-3051, American Institute of Aeronautics and Astronautics, Washington, D.C., Seattle, WA, 1997.

[19]Barral, S., "Theoretical Analysis of the Influence of the Power Supply on Breathing Oscillations in Hall Thrusters," *Proc. 30th International Electric Propulsion Conference*, No. 07-261, The Electric Rocket Propulsion Society, Worthington, OH, Florence (Italy), 2007.

[20]Barral, S. and Ahedo, E., "Low-Frequency Model of Breathing Oscillations in Hall Discharges," *Phys. Rev. E*, Vol. 79, 2009, pp. 046401.

[21]Barral, S. and Peradzyński, Z., "A New Breath for the Breathing Mode," *Proc. 31st International Electric Propulsion Conference*, No. 09-070, The Electric Rocket Propulsion Society, Worthington, OH, Ann Arbor, MI, 2009.